Durability of Reinforced Concrete Structures with externally bonded FRP Sheets

T. Shimomura & K. Maruyama
Nagaoka University of Technology, Niigata, Japan

ABSTRACT: This study focuses on long-term performance of reinforced concrete structures with externally bonded FRP sheet, which is carbon or aramid textile bonded with epoxy resin. Laboratory tests were carried out to investigate the durability aspect of concrete member retrofitted with FRP sheet. It was experimentally verified that the FRP sheet can reduce chloride ingress into concrete. Diffusivity of chloride ions in the layer of FRP sheet was identified by the numerical analysis of the test results. It was clarified that FRP sheet can improve mechanical performance of deteriorated concrete members due to reinforcement corrosion and associated concrete crack. Consequently, retrofit of FRP sheet is effective to improve durability, i.e. to extend service-life, of existing concrete structures.

1 INTRODUCTION

In the last ten years, upgrading of existing concrete structures by externally bonded fiber reinforced plastic (FRP) sheet has been increasingly adopted in Japan (JCI 1998, JSCE 2001, Ueda et al 2001). Continuous fiber sheets, which are carbon or aramid fiber textiles, are bonded on the surface of existing concrete structures with epoxy resin. The principal purpose of this upgrading technique is to improve mechanical performance of existing concrete structures, namely load-carrying capacity and ductility. Therefore, most of research projects on FRP sheets so far were based on this point of view.

However, durability of concrete structures with FRP sheet has not yet been well clarified. Though residual service-life of the upgraded structure is often discussed in practical design, there has been no verification method for its durability. Considering this situation, this study focuses on durability of concrete structures with FRP sheet.

Since epoxy resin has originally very low permeability, FRP sheet bonded on concrete surface can protect concrete from ingress of aggressive agents, such as chloride ions, and consequently extend service-life of the structure. Permeability test of reinforced concrete (RC) specimens with FRP sheet was carried out to examine the effectiveness of FRP sheet to reduce chloride ingress into concrete, as well as to increase mechanical performance. Diffusion coefficient of chloride ions within FRP sheet was quantified from the test results and the numerical analysis.

On the other hand, FRP sheet is normally applied on existing structures under service. In most studies, sound concrete structures are considered without any fatal material deterioration. However, in actual existing concrete structures, material deteriorations, such as reinforcement corrosion or associated concrete crack, have been sometimes induced before retrofitting FRP sheet. In order to investigate the influence of reinforcement corrosion on strengthening of RC member by FRP sheet, uniaxial tensile tests of RC specimens were carried out in this study. Reinforcement corrosion and corrosion crack were induced in the laboratory. Tensile behavior of RC specimens with FRP sheet was examined.

Finally in this study, numerical simulation of performance of concrete structures after retrofitting FRP sheet is demonstrated as a function of time based on the knowledge obtained from the experiments.

2 DIFFUSIVITY OF CHLORIDE ION IN FRP SHEET WITH EPOXY RESIN

2.1 *Outline of experimental study*

It is difficult to measure the diffusivity of aggressive agents, such as chloride ions or water, within the layer of epoxy resin on the surface of concrete under the normal condition because epoxy resin has very low permeability and may hardly allow chloride ingress. Therefore, the electrical permeability test was employed (Shimomura et al 2004).

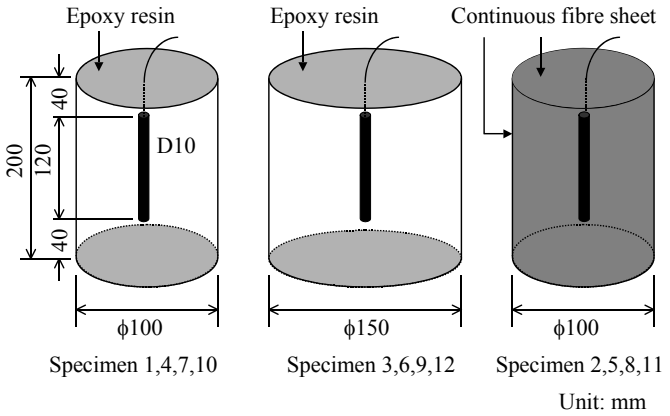

Figure 1. Cylindrical specimen for permeability test

Table 1. Conditions of specimens

Specimen No.	W/C of concrete (%)	Thickness of cover (mm)	FRP sheet wrapping
1	60	45	No
2	60	45	Yes
3	60	70	No
4	50	45	No
5	50	45	Yes
6	50	70	No
7	40	45	No
8	40	45	Yes
9	40	70	No
10	30	45	No
11	30	45	Yes
12	30	70	No

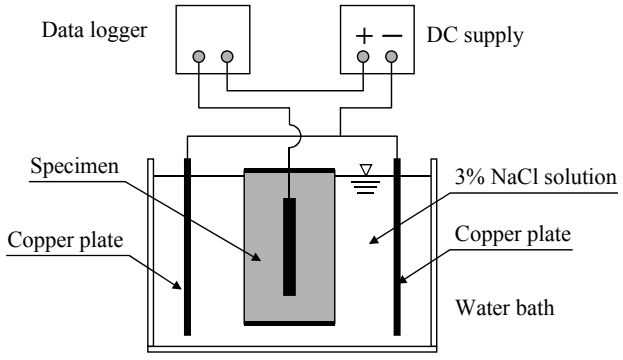

Figure 2. Setup for chloride permeability test

Cylindrical concrete specimens shown in Figure 1 were used in the test. Twelve specimens, whose experimental parameters are water-cement ratio of concrete, thickness of concrete cover and wrapping of carbon FRP sheet on the surface, were tested. Testing conditions of the specimens are indicated in Table 1.

Setup for the permeability test is shown in Figure 2. Constant electric voltage of 30V was applied to the specimen in NaCl solution. Time-dependent direct current penetrating the concrete was measured.

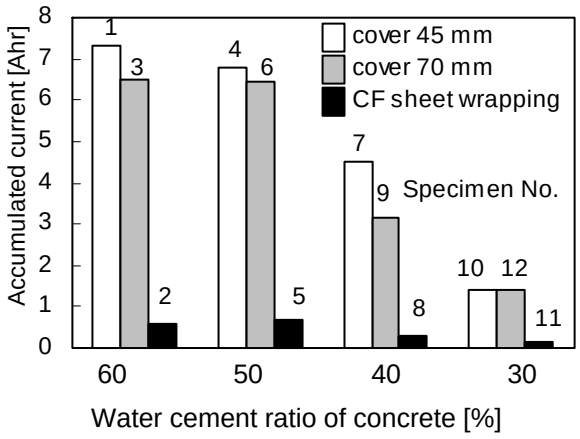

Figure 3. Accumulated electric current of the specimens until 90 hours

2.2 *Test results*

Concrete cracks were generated in the specimens 1 and 4 around 100 hours by corrosion of reinforcements in concrete. Electric resistance of concrete cover was suddenly lost after cracking. In order to compare permeability of all the specimens under the unified condition, therefore, accumulated electric current until 90 hours is taken as an index for permeability of specimen as shown in Figure 3.

Comparing the obtained accumulated electric current without FRP sheet in Figure 3, it is clear that permeability of concrete decreases with decreasing of water-cement ratio and increasing of thickness of concrete cover. These tendencies are very reasonable. In cases that FRP sheet is attached on the surface of concrete, accumulated current became very small in spite of water-cement ratio of concrete. It is verified that the system of FRP sheet and epoxy resin is effective as a surface insulator against ingress of materials into concrete.

2.3 *Numerical analysis of transport of chloride*

The authors have developed a computational model for the transport process of water and chloride ions in concrete based on pore structure of concrete and thermodynamic behavior of water in porous media (Shimomura and Maekawa 1997, Shimomura and Maruyama 2000). Mass conservation equations of water and chloride are respectively expressed as follows:

$$\frac{\partial w}{\partial t} = -div\left(J_v + J_l\right) \tag{1}$$

$$\frac{\partial C_{Clt}}{\partial t} = -div\left(J_{Cldif} + C_{Clf}\frac{J_l}{\rho_l}\right) \tag{2}$$

where, w = mass concentration of water per unit concrete volume, t = time, and J_v and J_l = mass flux

of vapor and liquid water respectively, C_{Clt} = total mass concentration of chloride per unit concrete volume, J_{Cldif} = mass flux of chloride by molecular diffusion and C_{Clf} = mass concentration of free chloride. The last term in Equation (2) expresses mass flux of chloride ions carried by liquid water that can be obtained from the moisture transport analysis.

It is necessary to execute coupling analysis of water and chloride to evaluate transport of chloride in non-saturated concrete in the atmosphere. However, in case of saturated concrete, molecular diffusion is dominant as transport mechanism of chloride in concrete. The mass flux of chloride by molecular diffusion is formulated as:

$$J_{Cldif} = -K_{Cl} D_{Cl} \, grad \, C_{Clf} \tag{3}$$

where, K_{Cl} = non-dimensional material factor of concrete as a function of its pore structure, D_{Cl} = diffusivity of chloride ion in liquid water.

Mass flux of chloride by molecular diffusion at the boundary surface is formulated as:

$$J_{Cldif} = -D_{Cl} \frac{C_{Clf}(0) - V_o \cdot C_{ext}}{h_{Cl}} \tag{4}$$

where, $C_{Clf}(0)$ = mass concentration of free chloride in concrete at the surface, V_o is porosity of concrete, C_{ext} is mass concentration of chloride in external solution and h_{Cl} is thickness of boundary-layer for mass concentration of chloride, in which local gradient of mass concentration of chloride is developed as shown in Figure 4.

When FRP sheet is bonded on the surface of concrete with epoxy resin, mass flux of chloride through the sheet is calculated as:

$$J_{Cldif} = -D_{cf} \frac{C_{CLf}(0) - V_o \cdot C_{exy}}{t_{cf}} \tag{5}$$

where, D_{cf} = diffusion coefficient of chloride ion in the layer of FRP sheet and epoxy resin and t_{cf} = thickness of the layer of FRP sheet and epoxy resin. Profile of mass concentration of chloride near the boundary is schematically shown in Figure 4.

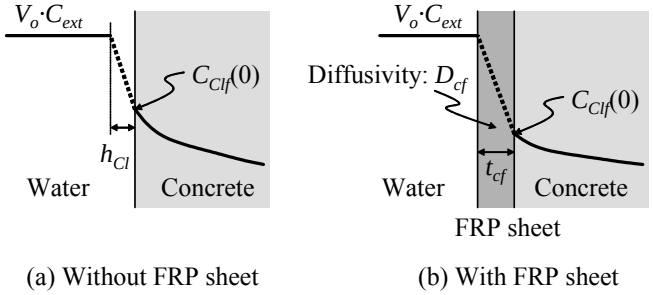

(a) Without FRP sheet (b) With FRP sheet

Figure 4. Profile of mass concentration of chloride near the boundary

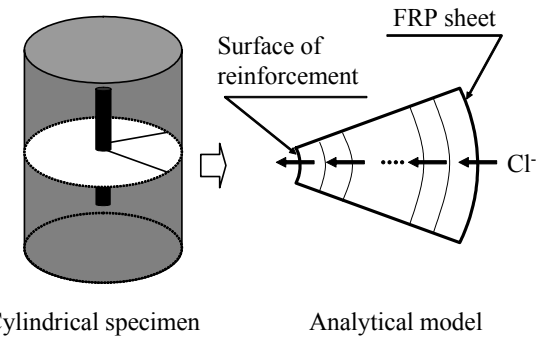

Figure 5. Numerical analysis of transport of chloride ion in cylindrical specimen

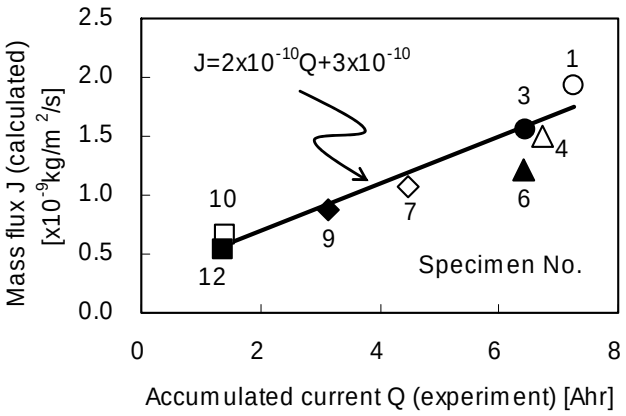

Figure 6. Correlation between the experimental and the analytical results

2.4 *Evaluation of diffusion coefficient*

Diffusion processes of chloride in the cylindrical concrete specimens that were used in the electric permeability test were analyzed by the proposed diffusion model. Finite differential method was employed to solve the governing equations numerically (Figure 5).

Material parameters for concrete were determined based on the previous study (Shimomura and Maekawa 1997). The driving force in the experiment is the gradient of electric potential, while the driving force assumed in the computational model is the gradient of chloride concentration. Though they are different phenomena in fact, these two transport phenomena may have some correlation with each other since they are both transport phenomena of ions in concrete. Hence, before discussing permeability of FRP sheet, the correlation between the experiment and the analysis is verified using the results of the specimens without FRP sheet (Figure 6).

Figure 6 shows the relationship between the experimental and the analytical results performed in this study. Accumulated electric current until 90 hours (Q) is taken as the index of the experimental result, while mass flux of chloride in the steady state (J) is taken as the index of the analytical result. It is clear that the experimental results (Q) and the analytical ones (J) have good correlation in spite of wa-

ter-cement ratio of concrete and thickness of concrete cover. This result implies that the hypothesis on the correlation between the experiment and the analysis is correct. In Figure 6, an empirical equation between the experimental results (Q [Ahr]) and the analytical ones (J [kg/m^2/s]) is indicated.

$$J = 2\times10^{-10}Q + 3\times10^{-10} \quad \left(kg/m^2/s\right) \tag{6}$$

It is assumed that this empirical correlation may be adapted to the specimens with FRP sheet. Then, diffusion coefficient of FRP sheet can be determined by trial and error so that the obtained analytical result (J) and the experimental result of the specimen (Q) satisfy the empirical equation. In the analysis, the thickness of FRP sheet (t_{cf}) was set 1 mm.

The diffusion coefficients of FRP sheet, which were obtained by this method from the experimental results of the specimens with FRP sheet, are shown in Table 2. Close values were obtained from the four specimens. The obtained diffusion coefficient of FRP sheet was approximately 3x10^{-14}m^2/s.

Table 2. Diffusion coefficient of FRP sheet

Specimen No.	W/C of concrete (%)	Experimental Q (Ahr)	D_{cf} (x10^{-14}m^2/s)
2	60	0.56	2.29
5	50	0.68	2.99
8	40	0.28	3.03
11	30	0.13	4.69

3 STRENGTHENING RC MEMBER WITH REBAR CORROSION BY FRP SHEET

3.1 *Outline of experimental study*

Figure 7 shows the dimensions of reinforced concrete specimens with and without continuous fiber sheet (Shimomura et al 2003). Conditions of specimens are given in Table 3. The 100x100x1000 mm concrete prismatic specimens with single deformed steel bar (ϕ19mm) in their center were prepared. After casting of concrete, specimens were wrapped with wet cloths and had been kept in the laboratory room for four weeks.

After four weeks of curing, the specimens RC3 and RC4 were exposed to the electrolytic corrosion test. The test setup is shown in Figure 8. Only the corrosion length of the specimen, which is 800 mm at the middle of the specimen, was placed in a 3% NaCl solution, while the rest part of the specimen was kept out of the solution to ensure anchorage of the reinforcement at the ends of specimen by avoiding corrosion. Constant direct current of 0.7A was provided by a DC supply with an embedded reinforcement as an electrode.

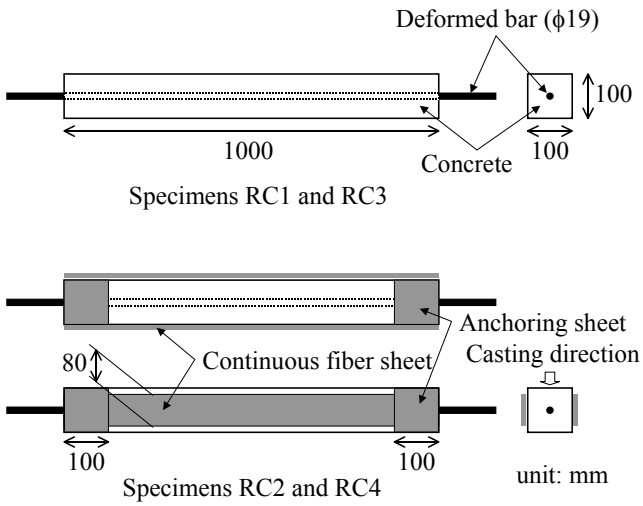

Figure 7. Specimens for uniaxial tensile test

Table 3. Condition of specimens

Specimen	Corrosion	FRP sheet
RC1	No	No
RC2	No	Yes
RC3	Yes	No
RC4	Yes	Yes
Bare bar A	No	-
Bare bar B	Yes	-

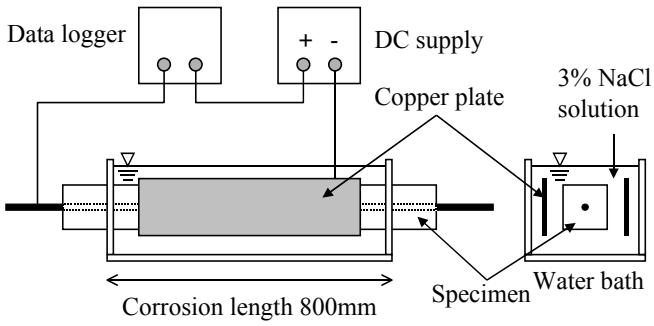

Figure 8. Test setup for electrolytic corrosion test

The corrosion test was continued until the cumulative current reaches the target value, which was set according to the previous test data (Matsuo et al 2001) so that the average corrosion in the corrosion length is about 1 mg/mm^2. In fact, longitudinal corrosion crack was observed at one of the concrete surface in both specimens after the electrolytic corrosion test. Actual amount of corrosion were measured by weight of the reinforcements taken out from the concrete after the loading tests. Electrolytic corrosion test of bare steel bar specimen B was also carried out with the same amount of cumulative current

Carbon FRP sheets were bonded on the two side surfaces of the specimens RC2 and RC4 as shown in Figure 7. The sheets on RC4 were bonded just after curing of concrete, while the sheets on RC4 were bonded after the electrolytic corrosion test. One of the sheets on RC4 was bonded just over the longitudinal corrosion crack that had been induced by the

corrosion test. Before bonding the sheets, the concrete surface was chipped and coated with a primer. Thereafter, the continuous fiber sheets were bonded with an epoxy resin.

As shown in Figure 7, anchoring sheets of 100 mm width were wrapped in both ends of the specimen to avoid delaminating of the longitudinal sheets from the ends. Aramid FRP sheets were used as the anchoring sheets because of their high flexibility.

The test setup for the uniaxial tensile test is shown in Figure 9. Tensile force was applied in the vertical direction in order to avoid eccentric load due to gravity as much as possible. Average strain of specimen was calculated from displacements measured with LVDT at the upper and bottom ends of the specimen. Local strains of continuous fiber sheets were measured with strain gages attached every 50 mm. Monotonic tensile force was applied. Tensile tests of the bare bar specimens A and B were also performed with this test setup.

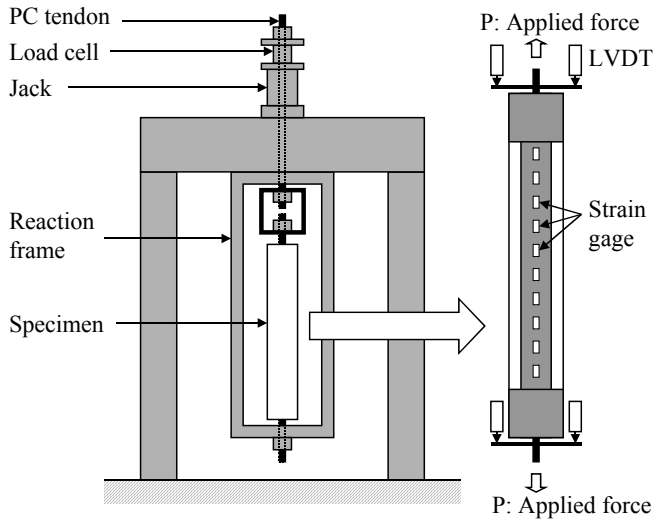

Figure 9. Test setup for uniaxial tensile test

3.2 *Formulation*

At an arbitrary section of a uniaxial specimen, applied force is carried by reinforcement, concrete and FRP sheets:

$$P = P_s(x) + P_c(x) + P_{cf}(x) \tag{7}$$

where, P = applied force, $P_s(x)$ = force carried by reinforcement at section x, $P_c(x)$ = force carried by concrete at section x and $P_{cf}(x)$ = force carried by FRP sheets at section x. $P_s(x)$, $P_c(x)$ and $P_{cf}(x)$ vary with respect to x because of concrete cracks and delaminating of sheets due to loading. By integrating Equation (7) with respect to x from the one end of the specimen to the other and dividing it by the length of the specimen, we obtain:

$$P = P_s + P_c + P_{cf} \tag{8}$$

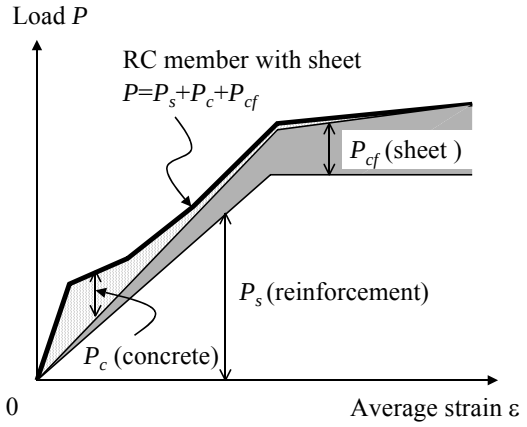

Figure 10 Load-sharing in RC member retrofitted with FRP sheet

Table 4. Mechanical properties of reinforcement

	Corrosion (mg/mm^2)	A_sE_s (kN)	Yielding force (kN)	A_s (mm^2)
Bare bar A	0	54500	97.8	286.5*
Bare bar B	1.18	44700	94.2	277.5**
Bar in RC3	1.27	-	-	276.8**
Bar in RC4	1.12	-	-	277.9**

* Nominal cross sectional area
** Calculated from nominal cross sectional area and loss of cross section estimated from corrosion

where, P_s = average force of reinforcement, P_c = average force of concrete and P_{cf} = average force of FRP sheets. By dividing P_s, P_c and P_{cf} by corresponding cross sectional areas, we obtain average stress of reinforcement, concrete and FRP sheet in RC member respectively.

Figure 10 illustrates the state of load sharing of reinforcement, concrete and sheet in a RC member with FRP sheet. In the conducted uniaxial tensile tests, applied force (P) and average strain (ε) of specimens were measured.

When the reinforcement is not yielding at any points, average force of reinforcement (P_s) is given by:

$$P_s = A_s E_s \varepsilon_s \tag{9}$$

where, A_s = cross sectional area of reinforcement, E_s = elastic modulus of reinforcement and ε_s = average strain of reinforcement. The products of cross sectional area and elastic modulus of reinforcement (A_sE_s) in both corroded and non-corroded specimens were determined based on the tensile tests of bare steel bars. The results are shown in Table 4.

The amount of corrosion in the specimens RC3 and RC4 indicated in Table 4 were directly measured from the reinforcements taken out from concrete after the loading tests. As these measured amounts of corrosion were found to be close to that of the bare bar B, the value A_sE_s of the bare bar B is adopted in computing the specimens RC3 and RC4. Average strain of reinforcement (ε_s) in Equation 9 is

assumed to be equivalent to average strain of specimen (ε), which was measured in the experiment. Since Equation 9 is true when reinforcement is in elastic stage, test data only before yielding are used in the computation in this study.

As FRP sheet is elastic material, its average force (P_{cf}) is given by:

$$P_{cf} = A_{cf} E_{cf} \varepsilon_{cf} \tag{10}$$

where, A_{cf} = cross sectional area of FRP sheet, E_{cf} = elastic modulus of FRP sheet and ε_{cf} = average strain of FRP sheet. Though the distribution of sheet strain is not uniform after cracking, average values always satisfy Equation 10 independently of strain distributions. In the computation, average value of measured strain distribution of sheet is used as ε_{cf}.

Consequently, we can calculate P_s and P_{cf} from measured values. Substituting them into Equation 8, we obtain average force of concrete (P_c) or average stress of concrete (σ_c):

$$\sigma_c = \frac{P - P_s - P_{cf}}{A_c} \tag{11}$$

where, A_c = cross sectional area of concrete.

3.3 *Test results and discussion*

Figure 11 shows obtained relationships between the applied force and the average strain of all the uniaxial test specimens. Concrete strengths at the age of loading test were between 27 and 30 N/mm^2.

The specimen RC1 is the standard one for comparison, which has neither reinforcement corrosion nor continuous fiber sheet.

The specimen RC2, which was strengthened with FRP sheets, had high stiffness than RC1 after cracking in concrete. Total applied load in RC2 increased even after yielding of reinforcement because FRP sheet is an elastic material.

The specimen RC3 with reinforcement corrosion had an apparent low stiffness from the initial stage. This is because cross sectional area of reinforcement was reduced due to corrosion.

The specimen RC4 showed almost same load-strain curve with RC2 though the reinforcement in RC4 had been corroded, while RC2 had no corrosion.

This result suggests that FRP sheets bonded on RC member cannot only simply strengthen the RC member but also recover the deterioration of mechanical performance of the RC member due to reinforcement corrosion. This possibility shall be investigated more in detail in terms of stress carried by concrete in the specimens calculated from the experimental data.

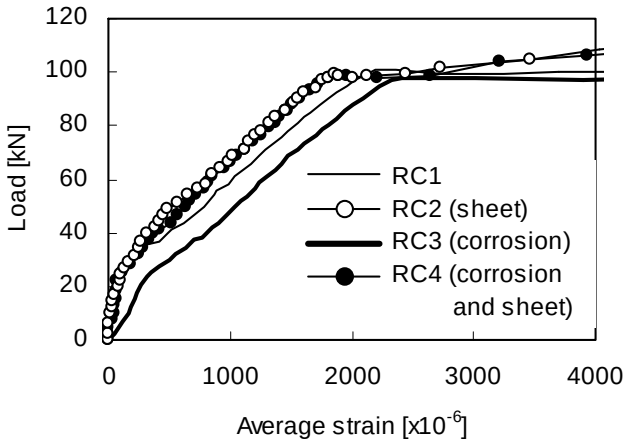

Figure 11. Load-strain curves for the uniaxial test specimens

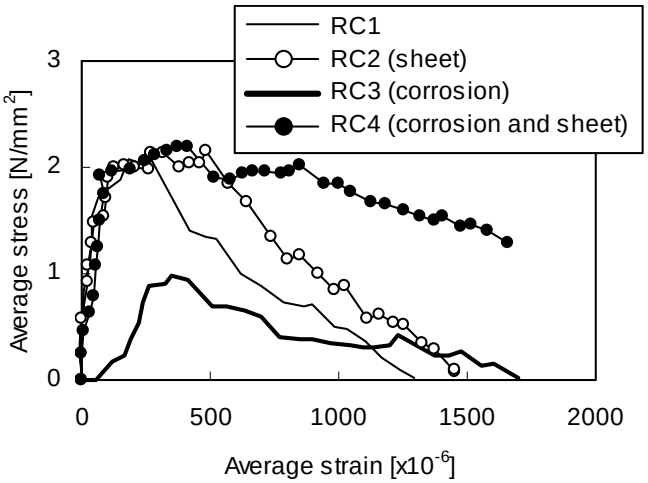

Figure 12. Average stress-strain curves of concrete

Figure 12 shows the average stress-strain curves of concrete in the four specimens. The average stress of concrete was calculated by Equation 11. The average strain was measured by LVDT.

Comparing the average stress-strain curves of RC1 and RC2 in Figure12, it is found that concrete stress increased when FRP sheet is retrofitted. The reason of this may be that bonding between concrete and reinforcement is improved because FRP sheet confines concrete externally. However, as the difference in the average stress-strain curves of RC1 and RC2 is small, the improvement of the tension-stiffness of concrete by FRP sheet may not be remarkable.

It is clear that the tension-stiffness of concrete in RC3 is smaller than that in RC1 because of reinforcement corrosion. Rust products on the surface of reinforcement and corrosion crack in concrete, both of which reduce bonding between concrete and reinforcement, may cause the degradation of the tension-stiffness of concrete.

4 NUMERICAL SERVICE-LIFE SIMULATION OF RC STRUCTURES WITH FRP SHEET

4.1 *Outline*

In order to verify the advantage of taking into account the insulating effect of FRP sheet as well as its strengthening effect in service-life prediction, numerical simulation of time-dependent performance change of reinforced concrete structure with FRP sheet was carried out. The flowchart of the calculation is shown in Figure 13. At each time step, chloride ingress into concrete, corrosion of reinforcement in concrete and load-carrying capacity of the member are calculated. As results, load-carrying capacity of the member is evaluated as a function of time. After retrofitting FRP sheet on the structure, its roles, as surface insulator and as external mechanical reinforcement, are taken into account on the basis of the experimental results shown in this paper.

4.2 *Analytical conditions*

Flexural capacity of RC beam with FRP sheet shown in Figure 14 under various conditions were calculated as a function of time. Material properties used in the analysis are shown in Table 5. Six cases were analyzed as indicated in Table 6.

The structure was assumed to stand under the corrosive environment with airborne salt from the sea. One-dimensional transport analysis was employed to evaluate chloride ingress into concrete as shown Figure 14. Corrosion of reinforcement in concrete caused by chloride and loss of cross-sectional area of the reinforcement due to corrosion were considered. Strengthening effect of FRP sheet was evaluated by the conventional beam theory. Delamination of the sheet was not considered.

Based on the experimental results shown in this paper, tension-stiffening effect of concrete cover is reduced as a function of corrosion of reinforcement. However, after FRP sheet is bonded on concrete, tension-stiffening effect of concrete cover is not reduced even if reinforcement is corroded.

4.3 *Results and discussion*

Figure 15 and 16 show the analytical results, in which flexural capacity of the beams as a function of time are plotted. In case 1, in which FRP sheet is not attached, flexural capacity of the beam decreases gradually because of reinforcement corrosion. In case 2, 3 and 4, in which FRP sheet is attached, flexural capacity is increased by the strengthening effect of the sheet and the time-dependent decreasing of flexural capacity is avoided by the insulating effect. The 'jump' in flexural capacity in the cases 3 and 4 in Figure 15 is attributable to the retrofitting of sheet.

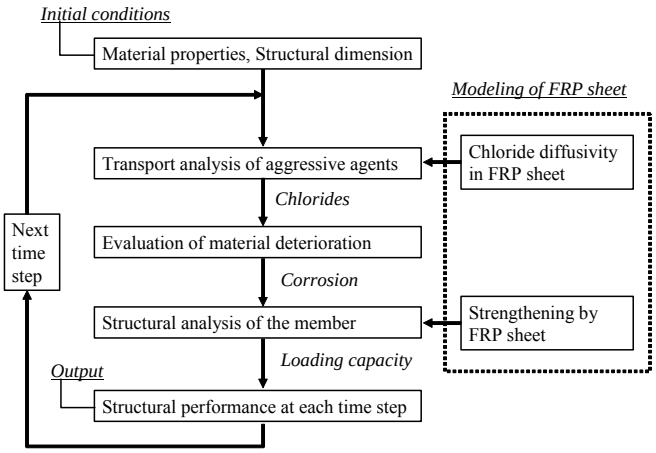

Figure 13. Flowchart of numerical service-life simulation of RC beam with FRP sheet

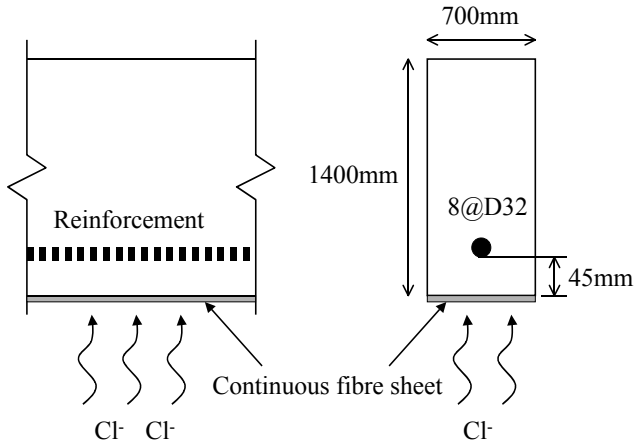

Figure 14. RC beam with FRP sheet

Table 5. Material properties

Concrete	
Unit water	165kg/m^3
Water-cement ratio	50%
Compressive strength	38N/mm^2
Other mechanical properties	Presumed from compressive strength
Parameters for mass transport	Presumed from mix proportion
Reinforcement	
Yield strength	400N/mm^2
Elastic modulus	200000N/mm^2
FRP sheet	
Thickness	1mm (including epoxy resin)
Tensile strength	3500N/mm^2
Elastic modulus	2.7x10^{5}N/mm^2
Diffusion coefficient	3x10^{-14}m^2/s

Table 6. Analytical cases

Case No.	Time of retrofit of FRP sheet	Effect of FRP sheet to be considered
1	without FRP sheet	-
2	from the initial stage	Insulating and strengthening
3	at 10 years	Insulating and strengthening
4	at 20 years	Insulating and strengthening
5	from the initial stage	Only insulating
6	from the initial stage	Only strengthening

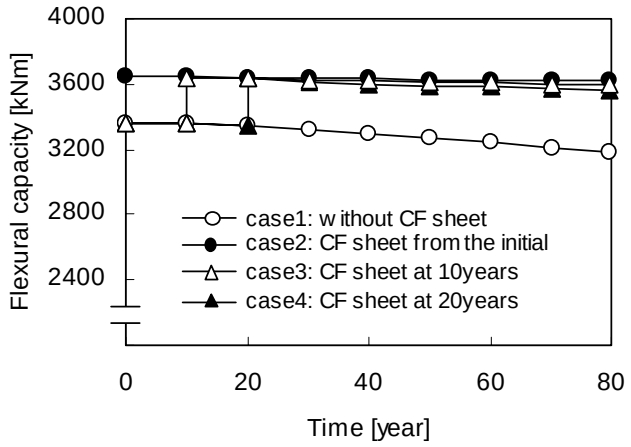

Figure 15. Analytical results 1: flexural capacity of beam as a function of time

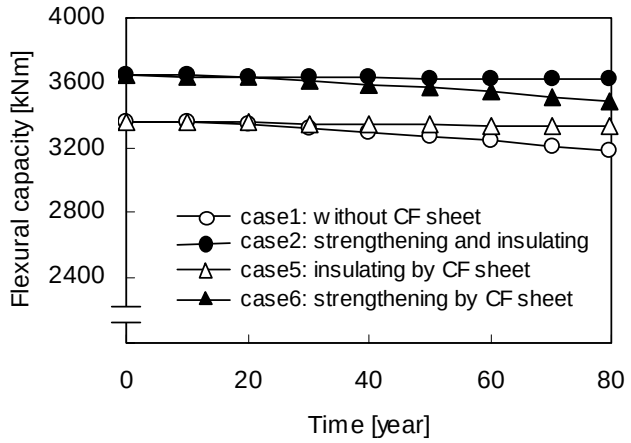

Figure 16. Analytical results 2: flexural capacity of beam as a function of time

As shown in Figure 15, the rate of deterioration after retrofitting of the sheet is a little different depending on the time of retrofitting. This is due to the difference of chloride concentration in concrete at the time of retrofitting.

The advantage to take into account the effectiveness of FRP sheet both as surface insulator and as external reinforcement is much clear in comparison of the results of case 1,2,5 and 6 in Figure 16. The flexural capacity in case 2, in which both effectiveness are taken into account, is kept the highest level among these four cases.

5 CONCLUSIONS

Concerning durability and service-life prediction of reinforced concrete structures with FRP sheet, following conclusions were obtained through this study.

The effectiveness of FRP sheet bonded on concrete to reduce chloride ingress was experimentally verified by the electric permeability test.

Coupling the electric permeability test and numerical diffusion analysis, diffusion coefficient of chloride in the layer of FRP sheet with epoxy resin was quantified.

FRP sheet bonded on concrete, as it is well-known, can strengthen the existing concrete member by carrying tensile stress. This strengthening mechanism of FRP sheet is effective both in sound member and deteriorated member by reinforcement corrosion.

FRP sheet bonded on concrete can recover the tension-stiffness of concrete that was once degraded by reinforcement corrosion. This recovery may be achieved by the confinement effect of FRP sheet on concrete.

Through the numerical service-life simulation of RC structure with FRP sheet, the advantage to take into account the effect of FRP sheet both as surface insulator and as external reinforcement was verified.

REFERENCES

Japan Concrete Institute. 1998. Technical Report on Continuous Fiber Reinforced Concrete.

Japan Society of Civil Engineers. 2001. Recommendations for Upgrading of Concrete Structures with Use of Continuous Fiber Sheets, Concrete Engineering Series 41

Ueda T., Shimomura T. and Maruyama K. 2001. Latest Design Method for Upgrading of Concrete Structures in Japan – JSCE Guidelines –, *Proceeding of the Eighth East Asia-Pacific Conference on Structural Engineering and Construction (EASEC8).*, *5-7 December 2001*. Singapore.

Shimomura T., Kasahara H. and Maruyama K. 2004, Numerical simulation of long-term behaviour of concrete structures with externally bonded continuous fibre sheet, *Proceeding of the International Conference on Advanced Polymer Composites for Structural Applications in Construction (ACIC2004)., 20-22 April 2004.* Guildford.

Shimomura T. and Maekawa K., 1997, Analysis of the drying shrinkage behaviour of concrete using a micromechanical model based on the micropore structure of concrete, *Magazine of Concrete Research*, 49(181): 303-322.

Shimomura T. and Maruyama K., 2000, Service life prediction of concrete structures subjected to chloride attack by numerical simulation, *Proceedings of the International RILEM Workshop on Life Prediction and Aging Management of Concrete Structures*, Cannes, RILEM Publications S.A.R.L.

Shimomura T., Kasahara H. and Okazaki M., 2003, Effectiveness of continuous fiber sheet in strengthening of reinforced concrete member with rebar corrosion, *Proceedings of the JCI International Symposium on Latest Achievement in Technology and Research on Retrofitting Concrete Structures -Interface Mechanics and Structural Performance*, Kyoto.

Matsuo H., Gokaku W. and Shimomura T., 2001, Tension Stiffness of Reinforced Concrete Member with Corroded Reinforcement, *Proceeding of the JCI*, 23(3), 1327-1332, (in Japanese).